

Reaction Model for Bituminous Coal Hydrogasification  
in a Dilute Phase

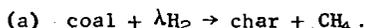
H. F. Feldmann, W. H. Simons,<sup>1/</sup> J. A. Mima, and R. W. Hiteshue

U.S. Bureau of Mines, 4800 Forbes Avenue  
Pittsburgh, Pennsylvania 15213

INTRODUCTION

Increasing demands and decreasing reserves of natural gas<sup>1,2/</sup> have intensified research and development efforts directed towards the production of supplementary pipeline gas. Several processes are currently being developed<sup>2/</sup> which will utilize our abundant fossil fuel reserves to meet the anticipated need for supplementary gas. One of these processes under investigation at the U.S. Bureau of Mines is the hydrogasification of raw bituminous coal to produce a pipeline quality gas consisting primarily of methane. There are certain features involved in the hydrogasification of raw bituminous coal which are economically and technically attractive: First, as shown by this study, the external hydrogen consumption required per unit of methane produced is low because of the efficient utilization of the hydrogen already in the coal; secondly, direct production of a high-Btu gas and use of a dilute-phase concurrent reactor (which minimizes agglomeration problems) are both possible because of the high reactivity which raw coal has for methane formation; and thirdly, process costs associated with pretreatment, inherent in other coal conversion processes based on bituminous coal feed stocks, are eliminated.

In this paper we describe a kinetic model for the overall reaction occurring in the hydrogasification reactor; that is



This model is being used in other studies to evaluate and optimize various types of hydrogasifier schemes as well as to predict by computer simulation temperature profiles in commercial sized reactors.

Most of our experimental data on the hydrogasification of coal comes from a reactor using concurrent gas-solids flow with the solids freely falling through the reactor. Although the primary reason for using this contacting system is to avoid agglomeration problems,<sup>3/</sup> this dilute-phase operation may also offer some advantages in temperature control because of the reduced heat generation per unit volume of reactor compared to moving bed or fluidized systems.

EXPERIMENTAL

Equipment and Procedure

The basic elements of the hydrogasification system are shown in figure 1. Hydrogen from a gasholder at atmospheric pressure is metered and compressed to reaction pressure in a 5-stage reciprocating compressor and is heated in tubing coiled around the reactor before being injected into the top of the reactor. Heat is supplied to the reactor and gas preheat coils with banks of individually controlled electric-resistance furnaces. Coal is fed to the reactor at system pressure using a 4-vaned feeder connected to a variable-speed motor; it passes by gravity flow through a nozzle of 5/16-inch diameter before entering the reactor. This nozzle is water-cooled to keep the coal below its softening temperature and is insulated to minimize heat losses. The coal is dispersed into the reactor where it contacts and reacts with the hydrogen. The reactor is of 3-inch inner diameter and the heated section below coal entry point has been varied from 3 to 6 feet in length. The coal must be heated very rapidly

<sup>1/</sup> Mathematician, Department of Mathematics, West Virginia University, Morgantown, West Va. 26506.

through its plastic temperature (350°-480° C for hvab coal, Pittsburgh seam) in order to produce a dry char, free of agglomerates. Residence time of volatile products varies with system pressure and gas rate but for most experiments made at 3,000 psig, this residence time runs about 5 minutes. Two types of reactors have been used for these experiments. For experiments made at 725°-750°C (EHR series), thick-walled stainless steel reactor with a 6-inch od x 3-inch id was used. For experiments at 900° C (IHR series), an internally-heated reactor was designed in which the reactor proper consists of 3-inch schedule 10 stainless steel pipe. The IHR reactor and heating elements are enclosed in a 10-inch pressure vessel and are insulated so that wall temperatures on this vessel do not exceed 150° C at reaction temperatures of 900° C. Equalized pressure is maintained across the wall of the 3-inch reactor.

Char is collected in an air-cooled receiver located below the reactor. Product gas passes through a water-cooled vessel in which water, traces of oil, and some volatile salts are condensed and collected. The gas is then expanded to atmospheric pressure through a regulator, metered, and flared. A separate sample stream, taken from a point near the bottom of the reaction zone, passes through a continuous analyzer that determines the concentration of hydrogen in the stream. Periodic samples are taken for complete analysis by chromatography. The char from the receiver is weighed and ultimate and proximate analyses made.

Experiments were made with hvab coal from the Pittsburgh seam having a free-swelling index of 8 and a volatile content of 39-41 percent, moisture-ash-free basis. Ultimate and proximate analyses are given in table 1. The feed was sized to 50 x 100 mesh sieve fraction, U.S. Standard.

Table 1.- Analyses of high-volatile A bituminous coal

|                            | As<br>received,<br>percent | Maf,<br>percent |
|----------------------------|----------------------------|-----------------|
| <b>Ultimate</b>            |                            |                 |
| Carbon .....               | 78.5                       | 84.0            |
| Hydrogen .....             | 5.4                        | 5.7             |
| Nitrogen .....             | 1.6                        | 1.7             |
| Sulfur .....               | 1.4                        | 1.5             |
| Oxygen <sup>1/</sup> ..... | 7.2                        | 7.1             |
| Ash .....                  | 5.9                        | -               |
|                            | 100.0                      |                 |
| <b>Proximate</b>           |                            |                 |
| Moisture .....             | 0.7                        | -               |
| Volatile matter .....      | 38.2                       | 40.9            |
| Fixed carbon .....         | 55.2                       | 59.1            |
| Ash .....                  | 5.9                        | -               |

<sup>1/</sup> By difference.

Development of Reaction Model

Ordinary methods of treating integral reactor data are not applicable to our data because, judging from product gas analyses, the system never reached steady state in the time allowed by the coal capacity of the pressurized hopper. The gas concentration versus operating time curves indicate substantial backmixing was occurring in the reactor and this backmixing was responsible for the delay in reaching steady state. A tracer experiment was conducted under controlled conditions and without the complications of chemical reactions to observe the precise behavior of the IHR reactor as a

mixer. In this experiment the hopper was charged with an inert solid (anthracite) and the same operating procedure was followed as in a run except that shortly after the start of feeding the anthracite, the hydrogen flow was turned off and inert gas fed in its place. The dimensionless concentration of nitrogen in the sample gas is shown in figure 2 as a function of time. These results indicate that based upon the so-called dispersion model,<sup>4</sup> the reactor may be treated as if the gas phase were perfectly mixed.

Because the reactor is backmixed and the residence time of the free-fall particles is short compared to the time over which a significant change in gas composition occurs, each particle entering the reactor sees an essentially constant gas composition while passing through the reaction zone. Of course, particles falling through the reactor at different operating times see different gas compositions so the char collected at the end of an experiment is a nonhomogeneous material composed of particles all of which experienced different reaction conditions. Thus, in the formulation of the hydrogasification model two time scales are necessary. The physical interpretation of these two time scales is illustrated by the following rate equation which was found to best fit the experimental data,

$$(1) \quad \partial z^*(t, \theta) / \partial \theta = k p_{H_2}(t) (1 - z^*),$$

where  $z^*$  is the carbon conversion at particle residence time  $\theta$  and at operating time  $t$ ,  $k$  is the reaction rate constant, and  $p_{H_2}(t)$  is the hydrogen partial pressure at operating time  $t$ . Since the measured carbon conversion,  $\bar{z}$ , is based on the total char collected, it is an average conversion and therefore may be assumed to be related to the instantaneous conversion by

$$(2) \quad \bar{z} t_R = \int_0^{t_R} z(t) dt,$$

where  $t_R$  is the duration of the run,  $z(t) = z^*(t, \theta_0)$  and  $\theta_0$  is the particle residence time.

Because the change in gas composition is negligible over a time span equal to the particle residence time  $\theta_0$ , equation (1) may be integrated with respect to  $\theta$  with  $t$  held constant. This yields

$$(3) \quad \int_E^{z(t)} dz^*(t, \theta) / (1 - z^*) = k p_{H_2}(t) \theta_0,$$

where the physical interpretation of  $E$  is the fraction of carbon that is immediately vaporized. From equation (3) and the definition  $\theta_0 = L/U_T$ , the carbon conversion of coal falling through the reactor at operating time  $t$  is given by

$$(4) \quad z(t) = 1 - (1 - E) \exp(-k p_{H_2}(t) L / U_T).$$

As previously mentioned, the solid carbon conversion measured is an average conversion so substitution of equation (4) into equation (2) gives

$$(5) \quad \bar{z} = 1 - (1 - E) / t_R \int_0^{t_R} \exp(-k p_{H_2}(t) L / U_T) dt$$

as the expression for the average solid carbon conversion over the run time  $t_R$ .

We have experimental values for  $\bar{z}$ ,  $t_R$ ,  $L$ ,  $p_{H_2}(t)$  as a discrete function of operating time  $t$ , and a rough estimate for  $U_T$  of 32,400 ft/hr at 205 atm. Equation (5) was used to correlate the hydrogasification data by the following steps:

1. Select a value for  $E$
2. For each experiment, with this  $E$  solve equation (5) for  $k$  by numerical methods.

3. Calculate the average k value for those experiments all performed at the same temperature, and using this k value in (5), calculate a  $\bar{z}$  for each of these experiments.

4. Determine the value of E that minimizes

$$\sum |\bar{z}_{\text{measured}} - \bar{z}_{\text{calculated}}|,$$

where the summation is taken over the experiments of step (3).

Results of experiments at the two temperature levels studied are shown with the feed conditions in table 2. For each temperature, the results presented in table 2

Table 2. - Tabulated reaction rate constants and reactor conditions

| IHR Run Series, T = 900° C, E = 0.14 |                        |                         |                                    |                           |   |                    |  |
|--------------------------------------|------------------------|-------------------------|------------------------------------|---------------------------|---|--------------------|--|
| Run                                  | Reactor pressure, atm. | Solids feed rate, lb/hr | Average solid carbon conversion, % | Gas feed rate, lb-mole/hr | Hydrogen in feed gas, vol%                                      | Reactor length, ft | Reaction <sup>2/</sup> rate constant k, atm <sup>-1</sup> hr <sup>-1</sup> |
| 36                                   | 205                    | 6.4                     | 31.0                               | 0.447                     | 1/48  | 5                  | 23.7   |
| 37                                   | 205                    | 13.6                    | 27.1                               | 0.550                     | 1/50  | 5                  | 21.4   |
| 38                                   | 205                    | 13.0                    | 22.0                               | 0.434                     | 1/45  | 5                  | 13.4   |
| 39                                   | 205                    | 13.2                    | 28.1                               | 0.695                     | 1/45  | 5                  | 21.0   |
| 61                                   | 205                    | 13.4                    | 26.0                               | 0.663                     | 1/50  | 5                  | 19.4   |
| 96                                   | 205                    | 4.3                     | 47.6                               | 0.329                     | 98  | 5                  | 19.2   |
| 101                                  | 205                    | 6.1                     | 49.6                               | 0.347                     | 96  | 5                  | 23.4   |
| 104                                  | 205                    | 6.9                     | 42.7                               | 0.363                     | 99  | 5                  | 16.7   |
| 107                                  | 205                    | 8.8                     | 53.0                               | 0.480                     | 99  | 5                  | 25.4   |
| 108                                  | 205                    | 7.2                     | 49.8                               | 0.450                     | 98  | 5                  | 24.0   |
| 109                                  | 205                    | 8.1                     | 47.8                               | 0.480                     | 98  | 5                  | 23.1   |
| 110                                  | 205                    | 8.2                     | 41.6                               | 0.468                     | 99  | 3                  | 27.5   |
| 111                                  | 205                    | 7.9                     | 39.8                               | 0.463                     | 99  | 3                  | 25.2   |
| 113                                  | 205                    | 8.3                     | 43.0                               | 0.405                     | 99  | 3                  | 21.7   |
| 129                                  | 205                    | 8.4                     | 40.0                               | 0.423                     | 100   | 5                  | 19.5   |
| 130                                  | 205                    | 8.1                     | 40.2                               | 0.437                     | 97  | 5                  | 18.8   |
| 131                                  | 205                    | 8.4                     | 42.0                               | 0.408                     | 96  | 5                  | 21.2   |
| 132                                  | 205                    | 8.8                     | 37.7                               | 0.432                     | 99  | 5                  | 14.3   |
| 133                                  | 205                    | 8.2                     | 40.5                               | 0.348                     | 99  | 5                  | 15.7   |
| 136                                  | 205                    | 7.8                     | 39.9                               | 0.447                     | 99  | 5                  | 17.8   |
| 125                                  | 69                     | 8.1                     | 36.8                               | 0.516                     | 97  | 5                  | 39   |
| 128                                  | 69                     | 8.2                     | 37.8                               | 0.368                     | 93  | 5                  | 43   |
|                                      |                        |                         |                                    |                           | Average k <sup>3/</sup> = 21 atm <sup>-1</sup> hr <sup>-1</sup> |                    |  |

1/ Except for about 2 vol pct the remainder of the gas is methane.

2/ Based on estimated average particle velocity of 32,400 ft/hr with char produced at 205 atm.

3/ Runs at 69 atm corrected for particle residence time for inclusion in average k.

(Table 2 continued on next page.)

Table 2-continued-

| EHR Run Series, T = 725° C, E = 0.22  |                       |                         |                                    |                           |                            |                    |  |
|---|-----------------------|-------------------------|------------------------------------|---------------------------|----------------------------|--------------------|--|
| Run   | Reactor pressure, atm | Solids feed rate, lb/hr | Average solid carbon conversion, % | Gas feed rate, lb-mole/hr | Hydrogen in feed gas, vol% | Reactor length, ft | Reaction <sup>2/</sup> rate constant k, atm <sup>-1</sup> hr <sup>-1</sup> |
| 346   | 205                   | 6.4                     | 22.8                               | 0.458                     | 1/58                       | 6                  | 5.89   |
| 347   | 205                   | 6.3                     | 25.2                               | 0.458                     | 1/52                       | 6                  | 2.87   |
| 349   | 205                   | 6.6                     | 25.6                               | 0.466                     | 1/51                       | 6                  | 3.13   |
| 352   | 205                   | 5.3                     | 23.4                               | 0.458                     | 1/49                       | 6                  | 12.38  |
| 377   | 205                   | 6.0                     | 39.4                               | 0.478                     | 98                         | 6                  | 7.08   |
| 394   | 205                   | 6.2                     | 23.8                               | 0.416                     | 1/29                       | 6                  | 3.00   |
| 399   | 205                   | 6.4                     | 24.0                               | 0.548                     | 1/27                       | 6                  | 3.29   |
| Average k at 205 atm = 5.4 atm <sup>-1</sup> hr <sup>-1</sup>                                   |                       |                         |                                    |                           |                            |                    |  |
| 369   | 103                   | 6.3                     | 29.6                               | 0.461                     | 1/55                       | 6                  | 12.00  |
| 370   | 103                   | 6.7                     | 27.0                               | 0.461                     | 1/56                       | 6                  | 7.03   |
| 373   | 103                   | 5.9                     | 27.7                               | 0.455                     | 1/57                       | 6                  | 8.63   |
| 374   | 103                   | 7.6                     | 25.1                               | 0.463                     | 1/54                       | 6                  | 4.81   |
| 375   | 103                   | 6.0                     | 31.0                               | 0.455                     | 96                         | 6                  | 7.64   |
| 397   | 103                   | 6.5                     | 24.8                               | 0.422                     | 1/23                       | 6                  | 11.11  |
| 398   | 103                   | 6.7                     | 25.9                               | 0.548                     | 1/24                       | 6                  | 13.98  |
| 404   | 103                   | 6.5                     | 29.8                               | 0.950                     | 1/46                       | 6                  | 12.48  |
| Average k at 103 atm = 9.7 atm <sup>-1</sup> hr <sup>-1</sup>                                   |                       |                         |                                    |                           |                            |                    |  |
| Average k at 725° C corrected for residence time effects = 6 atm <sup>-1</sup> hr <sup>-1</sup> |                       |                         |                                    |                           |                            |                    |  |

1/ Except for about 2 vol pct the remainder of the gas is methane.

2/ Based on estimated average particle velocity of 32,400 ft/hr with char produced at 205 atm.

are those calculated using the value of E in step (4). These results indicate an effect of pressure on k; however, this is merely a residence time effect due to the dependency of the char density on the system pressure. This dependency is shown in figure 3 where the bulk density of the char is plotted as a function of the reactor pressure. Apparently, the hollow spheres of which most of the char consists are smaller when formed under higher pressure. Photographs of char in figure 4 show this bulk density difference. Correction for the change in bulk density and the corresponding particle residence time gives k values that are independent of pressure, and these are the average values reported in table 2.

There is considerably more spread in the calculated k values at 725° C than at 900° C for the following reasons: Extensive carbon conversion at 725° C is due to devolatilization because of relatively low k values, the short residence time (<1 sec) in free-fall, and the low hydrogen partial pressure due to the higher methane concentrations in the feed gas. Thus, in equation (3) z(t) is close to E, and therefore, small errors in z(t) and E generate large errors in k. In view of this inherent instability, the calculational scheme described above was carried out under the additional constraint that E be less than the lowest measured carbon conversion. A comparison of the measured values of carbon conversion with those predicted by the model using the average k is shown in figure 5.

An apparent activation energy is calculated by plotting  $\ln k$  versus  $1/T$  for the two temperature levels studied in figure 6. Also shown in figure 6 is a  $k$  value reported by Wen and Huebler<sup>5/</sup> using a coal-char and a  $k$  value calculated from data reported by Moseley and Paterson<sup>6/</sup> also on char hydrogasification. The apparent activation energy calculated from figure 5 is about 16 k cal/gram-mole carbon reacted. This is in basic agreement with a hydrogasification activation energy of 15 k cal reported by Zahradnik and Glenn.<sup>2/</sup>

#### Physical Interpretation of the Reaction Model

In this section we establish a physical basis for our reaction model, not only to gain confidence in the model but also to ascertain the limits of its applicability. In order to provide this physical basis we must rely on intuition and the experimental work of others even though the bulk of the latter was generated with coal-char as a feed material rather than coal.

We have already compared in figure 6 the temperature dependency of the rate constants calculated in this study with those reported or calculated from references 5, 6, and 7. This comparison is encouraging in the sense that it tells us what we intuitively would suspect; that is, the activation energies for the hydrogasification of coal and char are not greatly different. Another encouraging factor is the variety of reactor configurations and solid-gas contacting schemes employed in the studies used to calculate activation energies. For example, Moseley and Paterson<sup>6/</sup> used an entrained reactor for their studies, Wen and Huebler<sup>5/</sup> treated data generated in both a semiflow (fixed coal charge and flowing hydrogen) and continuous countercurrent tubular reactor. Moseley and Paterson's char data also indicate that the hydrogasification reaction rate constant decreases with increasing char preparation temperature and would thereby be expected to be highest for raw coal, as our data confirm.

Since Moseley and Paterson conducted their entrained reactor studies with excess hydrogen, the hydrogen partial pressure remains essentially constant; therefore, it is possible to calculate reaction rates in their entrained reactor because mixing patterns need not be considered. In figure 7, using a  $k$  value calculated from their data, the rates predicted by our model are compared with their experimentally measured rates at the various hydrogen partial pressures used in their studies. The goodness of the fit is a further indication that this reaction model can be used under a rather wide range of contacting schemes and reactor conditions.

Since, in this model, the hydrogasification rate is a function of temperature, hydrogen partial pressure, and carbon conversion level, we should establish a range for these variables over which the model applies. A very conservative estimate is obtained by simply restricting the variables to the range covered by the present experimental study. From a process viewpoint, the range of variables in this study, as shown in table 2, is sufficiently wide to cover most practical process situations. Thus, the model can be used to design most reactor systems without extrapolating beyond the range of experimental conditions.

Equation (1), which describes the rate of hydrogasification, has the simple physical interpretation that the coal particle consists of a number of reaction sites all equally accessible to hydrogen. The porous nature of coal-chars formed during hydrogasification (as shown by a cross sectional view of some typical char particles in figure 8), indicates that this interpretation is reasonable. The rate of reaction under these circumstances is given by

$$-\frac{1}{N_{s0}} \frac{dN_s}{d\theta} = k_{pH_2} \frac{N_s}{N_{s0}}$$

which can be directly written in terms of conversion as

$$dz/d\theta = k_{pH_2}(1-z).$$

Hitashue and co-workers conducted semiflow experiments<sup>8/</sup> at the rapid heating rates typical of continuous operation. Their results indicate that the number of so-called reaction sites  $N_{SO}$  capable of being converted in the relatively short residence times of free-fall operation are not equal to the number of carbon atoms in the coal. Data from reference 8 are plotted in figure 9 to show how the fraction of total carbon available for reaction at short residence times is increased by increases in temperature and hydrogen partial pressure. The increase in the amount of more highly reactive carbon with increasing temperature was also pointed out by Wen and Huebler.<sup>9/</sup> A fairly reasonable physical interpretation of this phenomena is that the carbon containing molecules in the coal are unstable at the hydrogasification temperatures and can either form molecules amenable to further hydrogenation by the addition of hydrogen to the solid phase or form more highly aromatic, and hence unreactive, structures by polymerization. This basic explanation of hydrogasification has also been postulated by both Moseley and Paterson<sup>6/</sup> and Zahradnik and Glenn.<sup>2/</sup> The material remaining after the highly reactive carbon is hydrogasified also hydrogasifies, but at a much lower rate. The kinetics of hydrogasification of this more unreactive carbon are currently being analyzed using the data in reference 8. Though the kinetic analysis of the hydrogasification of the more unreactive fraction of carbon is incomplete, it also seems to follow the basic rate law

$$\frac{dz}{d\theta} = k p_{H_2}^a (1-z),$$

where  $a$  is the yet undetermined order of the reaction with respect to hydrogen partial pressure.

Thus, hydrogasification of raw coal can be explained by assuming the existence of the following three types of carbon:

Type 1. The highly reactive solid carbon contained in side chains which is extremely easy to split off from the solid molecule. This is the fraction of carbon denoted by  $E$  in this report.

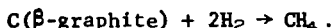
Type 2. The highly reactive solid carbon which readily hydrogasifies but at a lower rate than the carbon denoted by  $E$ . This is the fraction of carbon whose hydrogasification rate is described in this paper. As shown in figure 8, the fraction of reactive carbon depends on both the temperature and hydrogen partial pressure in the reactor.

Type 3. The low-reactivity residual carbon which seems to react according to the same rate law as type 2 but with a much lower value of  $k$ .

Alternate models based on char containing carbon of two different reactivities have been proposed by Wen and Huebler and Blackwood and McCarthy.<sup>7/</sup>

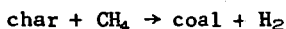
Our attention has thus far been focused on the solid carbon phase, and we should now consider the important role of the gaseous products on the hydrogasification reaction. One major effect of these gaseous products is, of course, the lowering of hydrogen partial pressure. Also, since the objective of these studies is to produce high-Btu gas, the maximum concentration of methane that can be produced and how it depends on the contacting scheme and reactor conditions should be determined. Our system is not a particularly good one for determining the maximum methane concentrations attainable because of the short solids residence time and the non-optimum solid-gas contacting system. In spite of these drawbacks, it is possible to produce a high-Btu gas after methanating the low concentrations of carbon monoxide to bring the gas into compliance with pipeline standards. For example, results of some experiments with hydrogen-methane feed gas at 900° C are presented in table 3. The feed gas composition used in these experiments comes from an experimental study<sup>10/</sup> which established the feasibility of a two-stage hydrogasification system in which the raw coal is contacted while in free-fall with the product gas coming from a moving-bed char hydrogasifier. Details of this system are given in reference 10 and reference 3.

Two important facts may be observed from the results in table 3. First, since the same hydrogasification rate expression applies to systems containing up to 80 mole-percent methane, the only effect of high methane concentrations is to reduce the partial pressure of hydrogen. (Zielke and Gorin<sup>11</sup> also report that in differential bed studies with methane-hydrogen gas mixtures and a Disco char, the only effect of methane is to reduce the hydrogen partial pressure.) Secondly, the experimentally measured group  $(Y_{CH_4}/Y_{H_2}P)$  is much higher than the equilibrium constant for the reaction



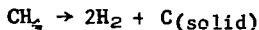
This is very important to process design because the relation between the partial pressures of methane and hydrogen and the solid carbon containing phase has been explained on thermodynamic grounds<sup>5,9,12,13</sup> as if there exists an equilibrium between a solid of changing activity level and the reacting species in the gas phase. This explanation leads to the experimentally unjustified conclusion that low temperatures (1,300° to 1,500° F)<sup>12</sup> are necessary to achieve the direct production of a high-Btu gas in continuous systems. Indeed, this thermodynamic analogy is causing concern regarding the feasibility of direct hydrogasification because it implies the necessity of removing heat from hydrogasification systems to maintain temperatures at the levels predicted by thermodynamic considerations to yield high-Btu gas. That these heat removal concerns are, at least at the present, unjustified is shown not only by the work reported here where 80 percent methane gas has been produced at temperatures of 900° C (1,652° F), but also by work reported by Birch and co-workers<sup>14</sup> on the hydrogasification of brown coal in a fluidized bed where large increases in both gasification rate and methane yield are obtained by increasing temperatures from 750° C to 950° C (1,742° F). So, based on presently available data, it appears that high-Btu gases can be produced at temperatures at least as high as 1,650° F. Kinetic studies at higher temperature are needed to determine whether heat removal from large reactors will be necessary or if it will simply suffice to provide wall cooling to protect materials of construction.

The danger in applying thermodynamic considerations (especially for extrapolational purposes) to hydrogasification systems becomes clear when one considers that the reactions involved in the production of methane from coal or char are not in any sense reversible and reversibility is a fundamental condition a system must satisfy to give the concept of equilibrium meaning. For example, the reaction



has never been known to occur. Therefore the behavior of hydrogasification systems must be considered to be dictated, at least to a large degree, by the kinetics of the above reaction.

A qualitative kinetic explanation for the behavior of hydrogasification systems is not difficult. For example, the generation of methane from raw coal or char can be represented by the rate equation developed in this paper which shows that the rate of methane formation increases exponentially with temperature up to the highest temperature studied (900° C). Figure 9 as well as data in reference 8 indicates that this increase in hydrogasification rate with temperature extends to 1,200° C. We have already seen that at 900° C methane/hydrogen ratios greatly exceed the ratio required for the formation of  $\beta$ -graphite and that the only effect of methane on hydrogasification rate even at these high methane levels is the reduction in hydrogen partial pressure. This simply means that the carbon deposition reaction



is slow compared to the formation rate of methane in spite of a thermodynamic driving force for the carbon deposition reaction. This could be due to a number of factors such as the lack of catalytic surfaces for deposition to occur on or their rapid poisoning by sulfur and/or nitrogen compounds in the coal.

Table 3.- Final product gas methane concentrations/ from the hydrogasification of raw coal with hydrogen-methane mixtures at 900° C

| IHR Run                       | 36   |         | 37   |         | 38    |         | 39    |         | 61   |         |
|-------------------------------|------|---------|------|---------|-------|---------|-------|---------|------|---------|
|                               | Feed | Product | Feed | Product | Feed  | Product | Feed  | Product | Feed | Product |
| H <sub>2</sub> ....           | 48.4 | 23.0    | 50.3 | 15.2    | 44.6  | 12.9    | 44.7  | 17.3    | 50.4 | 18.5    |
| CH <sub>4</sub> ...           | 47.7 | 73.0    | 46.0 | 78.7    | 51.6  | 81.1    | 52.1  | 77.9    | 45.3 | 75.5    |
| CO ....                       |      | 0.6     |      | 2.7     |       | 1.8     |       | 1.6     |      | 1.5     |
| CO <sub>2</sub> ....          |      |         |      | 0.2     |       | 0.7     |       |         |      |         |
| N <sub>2</sub> ....           | 3.8  | 3.3     | 3.6  | 2.9     | 3.8   | 3.3     | 3.2   | 2.9     | 4.2  | 4.3     |
| C <sub>2</sub> H <sub>6</sub> |      | 0.1     |      | 0.2     |       | 0.2     |       | 0.2     |      | 0.2     |
| Total <sub>2</sub> /          | 99.9 | 99.9    | 99.9 | 99.9    | 100.0 | 100.0   | 100.0 | 99.9    | 99.9 | 100.0   |

1/ These are experimental values and not the calculated steady state values.

2/ The difference between the total reported and 100 is due to a small amount of oxygen contamination of the samples.

Based on these kinetics, one suspects that the carbon deposition reaction would be most predominant at high carbon conversions, because of the low methane formation rates due to the influence of the  $(1-z)$  term, and at long gas phase residence times which give the methane formed time to crack. Both of these conditions can be minimized in continuous systems where carbon conversion levels will probably be on the order of 45 percent and the vapor phase residence time can be kept short. Thus, the continuous system may be able to operate at substantially higher temperatures and methane concentrations than batch systems without encountering appreciable carbon deposition.

#### Behavior of Experimental Reactor Using Model

Basically, what we have thus far developed is a model that allows the rate of conversion of carbon to be calculated when the environment of the char particles is known. In order to use this model to simulate reactor behavior, we must be able to establish the particle environment as a function of controllable reaction parameters. In the laboratory reactor described we can control feed gas rate  $G_0$ , coal feed rate  $W_{SO}$ , temperature  $T$  (in a larger adiabatic reactor the temperature would be a function of input variables rather than independently controllable), total pressure  $P$ , the composition of the inlet gas, and the length of the reactor (within certain limits). Since we have already established that the flow regime in our reactor is backmixed, the unsteady state methane flux in the reactor is described at operating time  $t$  by

$$(6) \quad G_0 y_{mo} - G y_m(t) + W_{SO} f_{CO} z(t) = \alpha V_R dy(t)/dt,$$

where  $G_0$  = feed gas rate,  $y_{mo}$  = concentration of methane in the feed gas,  $G$  = exit gas rate,  $y_m(t)$  = concentration of methane in the exit gas at time  $t$ ,  $W_{SO}$  = coal rate,  $f_{CO}$  = molar concentration of carbon in the coal,  $z(t)$  = coal carbon conversion level,  $\alpha$  = effective gas capacity of the reactor, and  $V_R$  = effective reactor volume. Substituting equation (4) into (6) and using the approximate empirical relation

$$y_{H_2}(t) = 0.98 - y_m(t),$$

for the methane-hydrogen mixtures used in these tests give

(7)  $G_0 y_{mo} - G y_m(t) + W_{SO} f_{CO} (1 - (1-E) \exp(-kP(0.98 - y_m(t))L/UT)) = \alpha V_R dy_m(t)/dt$ , which may be used to simulate unsteady state reactor behavior when  $G$  and  $\alpha$  are determined. The relation between  $G$  and  $G_0$  in terms of  $\lambda$ ,  $W_{SO}$ ,  $f_{CO}$ , and  $z$  is

$$(8) \quad G = G_0 - (\lambda - 1) W_{SO} f_{CO} z.$$

Figure 10 shows  $\lambda$ , as defined by equation (8), as a function of solid carbon conversion for the raw coal calculated two different ways. The curve determined by the experimental points is based on measured solid carbon conversion and the ratio of inlet/exit gas rates. Average residue and raw coal analyses were used to compute curves (a) and (b). Curve (a) assumes all the coal oxygen consumes hydrogen to form water; curve (b) assumes no hydrogen is consumed by the oxygen in the coal. Also shown are points based on data presented by Pyrcioch and Linden (15) as well as a few points from reference (5) both of which are based on the hydrogasification of pretreated coal. The difference between the curves for raw coal and pretreated coal is of primary economic importance because it reflects the difference in hydrogen consumption required to produce methane from the two feed stocks. The primary reasons for the difference in hydrogen consumption are the H/C atom ratio of the raw coal is about 0.83 while it is only about 0.52 for the pretreated coal and the oxygen content of the raw coal is lower.

As figure 10 indicates, for a raw coal feed at  $z < .45$   $\lambda = 1$  so under these conditions  $G = G_0$ . Equations (7) and (8) together with an estimate of  $\alpha$  may be used to simulate the behavior of the experimental reactor. Because of the internal construction of the IHR reactor used to test the simulation model, it is difficult to determine the effective volume for gas mixing and it was therefore necessary to find the value of  $\alpha$  from experimental data rather than calculating it from reactor volume, temperature, and pressure. The use of this technique to simulate a typical unsteady state performance of the experimental reactor with hydrogen feed is illustrated in figure 11 by comparing the predicted methane concentration with that measured. Figure 12 shows the simulation of the unsteady state period of some runs using a hydrogen-methane feed gas. Results in figures 11 and 12 indicate that the reactor approaches steady state quicker with hydrogen-methane mixtures than with hydrogen alone. The reason for the lowering of  $\alpha$  with increasing methane concentration, which is also indicated in figure 11, is not known but might be due to either the increased density of the gas, causing less transfer of hydrogen-rich hopper gas into the sample system, or due to the lower diffusivity of the mixture which would also result in less transfer between the reactor and insulating shell. Thus, average values of  $\alpha$  may be calculated from experimental data and the average  $\alpha$  together with equations (7) and (8) can be used to simulate unsteady state behavior of the reactor. However, while simulation of the unsteady-state behavior of the reactor is useful in that it lends credibility to the model, establishes the operating time necessary to approach steady state, and allows experiments to be simulated at conditions not experimentally attainable, it is the steady state behavior of the reactor that is most important. Calculation of steady-state operating parameters is accomplished by simply setting  $dy_m(t)/dt = 0$  in equation (7). Steady state behavior in terms of input parameters is then summarized by

$$(9) \quad G_0 y_{m0} - y_{ms} (G_0 - (\lambda - 1) W_{so} f_{CO} z_s) + W_{so} f_{CO} (1 - (1 - E) \exp(-kP(0.98 - y_{ms})L/UT)) = 0,$$

and

$$(10) \quad z_s = 1 - (1 - E) \exp(-kP(0.98 - y_{ms})L/UT),$$

where the subscript s refers to steady state conditions.

#### CONCLUSIONS

A reaction model for the hydrogasification of raw bituminous coal has been developed. This model is shown to be physically reasonable and to allow for the correlation of char hydrogasification data as well as the data for raw coal. The hydrogasification data indicates that the solid carbon reacts with hydrogen in three definite modes each of which has a different reactivity than the preceding.

The hydrogasification of raw coal is found to have two processing advantages over coal-chars in addition to the savings in pretreatment cost. These are a considerably higher hydrogasification rate than coal-chars and a much lower hydrogen consumption to produce a unit of methane.

Finally, the thermodynamic analogue, which has been widely used to predict desirable conditions for high methane concentrations in hydrogasification processes, is questioned and an alternate approach via kinetics is suggested as a means of determining the relationships between concentrations of gas phase species and the solid phase.

#### SUMMARY OF NOTATION AND UNITS

$\theta$  = the particle residence time at any point in the reactor, hr.

$\theta_0$  = the particle residence time at the reactor exit, hr.

$t$  = the operating time defined as  $t = 0$  when the coal feed starts and  $t = t_R$  when the coal feed is terminated, hr.

$z^*$  = the instantaneous solid carbon conversion at any point in the reactor,  $z^* = z^*(t, \theta)$ .

$z(t)$  = the instantaneous carbon conversion at the reactor exit,  $z(t) = z^*(t, \theta_0)$ .

$\bar{z}$  = the integrated average solid carbon conversion over the run time  $t$ .  
 $z_s$  = the steady state solid carbon conversion level.  
 $k$  = the reaction rate constant,  $\text{atm}^{-1}\text{hr}^{-1}$ .  
 $p_{\text{H}_2}(t)$  = the hydrogen partial pressure in the reactor at time  $t$ , atm.  
 $P$  = total reactor pressure, atm.  
 $L$  = reactor length, ft.  
 $U_T$  = particle terminal velocity, ft/hr.  
 $E$  = fraction of carbon in coal that is immediately devolatilized.  
 $N_s$  = number of carbon atoms in coal,  $N_s = f(t, \theta)$ .  
 $N_{s0}$  = initial number of carbon atoms in coal.  
 $y_m(t)$  = mole fraction of methane in exit gas at operating time  $t$ .  
 $y_{m0}$  = mole fraction of methane in feed gas.  
 $y_{ms}$  = mole fraction of methane in exit gas at steady state.  
 $y_{\text{H}_2}(t)$  = mole fraction of hydrogen in feed gas at operating time  $t$ .  
 $G_0$  = gas feed rate, lb-mole/hr.  
 $G$  = exit gas rate, lb-mole/hr.  
 $W_{s0}$  = coal feed rate, lb/hr.  
 $f_{\text{CO}}$  = carbon content of coal feed, lb-mole/lb-coal.  
 $V_R$  = effective volume of reactor, cu ft.  
 $\alpha$  = effective reactor gas capacity, lb-mole/cu ft reactor.  
 $\lambda$  = a stoichiometric coefficient.

#### REFERENCES

1. Liversidge, A. Not Enough Gas in the Pipelines. *Fortune*, November 1969; pp. 120-122, 189-190.
2. A Staff Report on National Gas Supply and Demand. Federal Power Commission, Bureau of Natural Gas, Washington, D.C., September 1969.
3. Hiteshue, R. W. The Hydrogasification of Raw Bituminous Coal. Proceedings of the Synthetic Pipeline Gas Symposium, Pittsburgh, Pa., Nov. 15, 1966, pp. 13-23.
4. Levenspiel, O. Chemical Reaction Engineering. John Wiley and Sons, New York, 1962, pp. 261-264.
5. Wen, C. Y. and J. Huebler. Kinetic Study of Coal-Char Hydrogasification - Rapid Initial Reaction. I. & E.C. Process Design and Development, v. 4, No. 2, April 1965, pp. 142-147.
6. Moseley, F. and D. Paterson. The Rapid High-Temperature Hydrogenation of Coal-Chars Part 2: Hydrogen Pressures up to 1,000 Atmospheres. *J. Inst. of Fuel*, Sept. 1965, pp. 378-391.
7. Zahradnik, R. L. and R. A. Glenn. The Direct Methanation of Coal. Fuel Division preprints of the 158th National A.C.S. Meeting, New York, N.Y., Sept. 7-12, 1969, pp. 52-70.
8. Hiteshue, R. W., S. Friedman, and R. Madden. Hydrogasification of High-Volatile A Bituminous Coal, BuMines Rept. of Inv. 6376, 1964.
9. Blackwood, J. D. and D. J. McCarthy. The mechanism of Hydrogenation of Coal to Methane, *Australian Journal of Chemistry*, 1966, 19, 797-813.
10. Lewis, P. S., S. Friedman, and R. W. Hiteshue. High-Btu Gas by Direct Conversion of Coal. Fuel Gasification, Advances in Chemistry 69, A.C.S. Publications, 1967.

11. Zielke, C. W. and E. Gorin. Kinetics of Carbon Gasification. I. & E. C., v. 47, No. 4, April 1955, pp. 820-825.
12. Feldkirchner, H. L. and J. Huebler. Reaction of Coal With Steam-Hydrogen Mixtures at High Temperatures and Pressures. I. & E. C., Process Design and Development, v. 4, No. 2, April 1965, pp. 134-142.
13. Dent, F. J. The Hydrogenation of Coal to Gaseous Hydrocarbons. International Conference on Complete Gasification of Mined Coal, Liege Belgium, May 3-5, 1954.
14. Birch, T. J., K. R. Hall and R. W. Urie. Gasification of Brown Coal With Hydrogen in a Continuous Fluidized-Bed Reactor. J. Inst. Fuel, Sept. 1960, pp. 422-435.
15. Pyrcioch, E. J. and H. R. Linden. Pipeline Gas by High-Pressure Fluid-Bed Hydrogasification of Char. I. & E. C., v. 52, No. 7, July 1960, pp. 590-594.

#### ACKNOWLEDGMENT

The authors express their appreciation to Miss Cynthia Deitz of West Virginia University for her help in the preparation of the computer programs which were used in this paper.

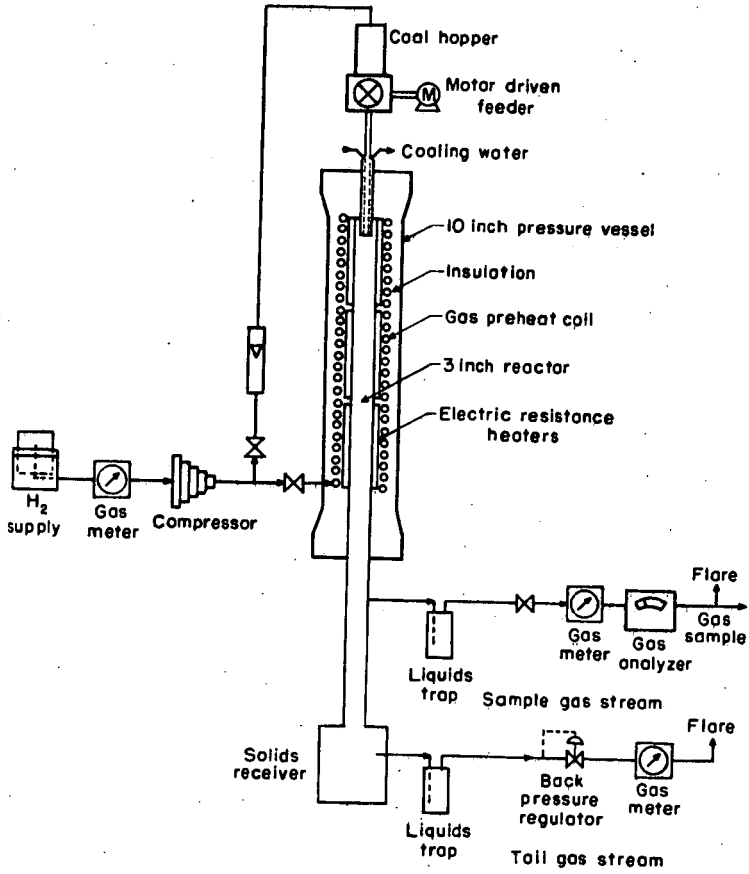


Figure 1—Schematic flowsheet for hydrogasification of coal in dilute phase.

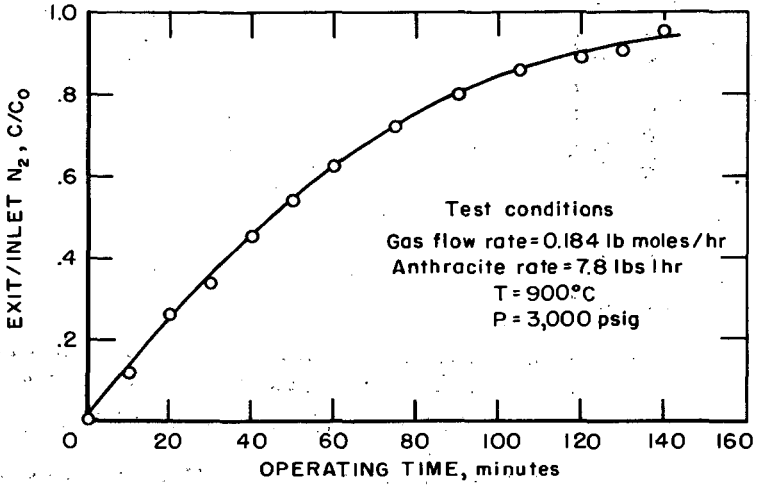


Figure 2—Behavior of the IHR reactor as a mixing vessel

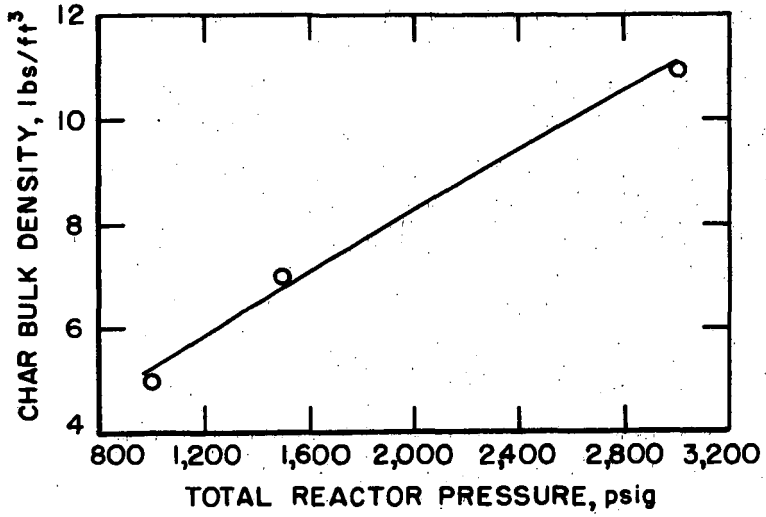


Figure 3-Effect of total reactor pressure on the bulk density of char produced by hydrogasification.

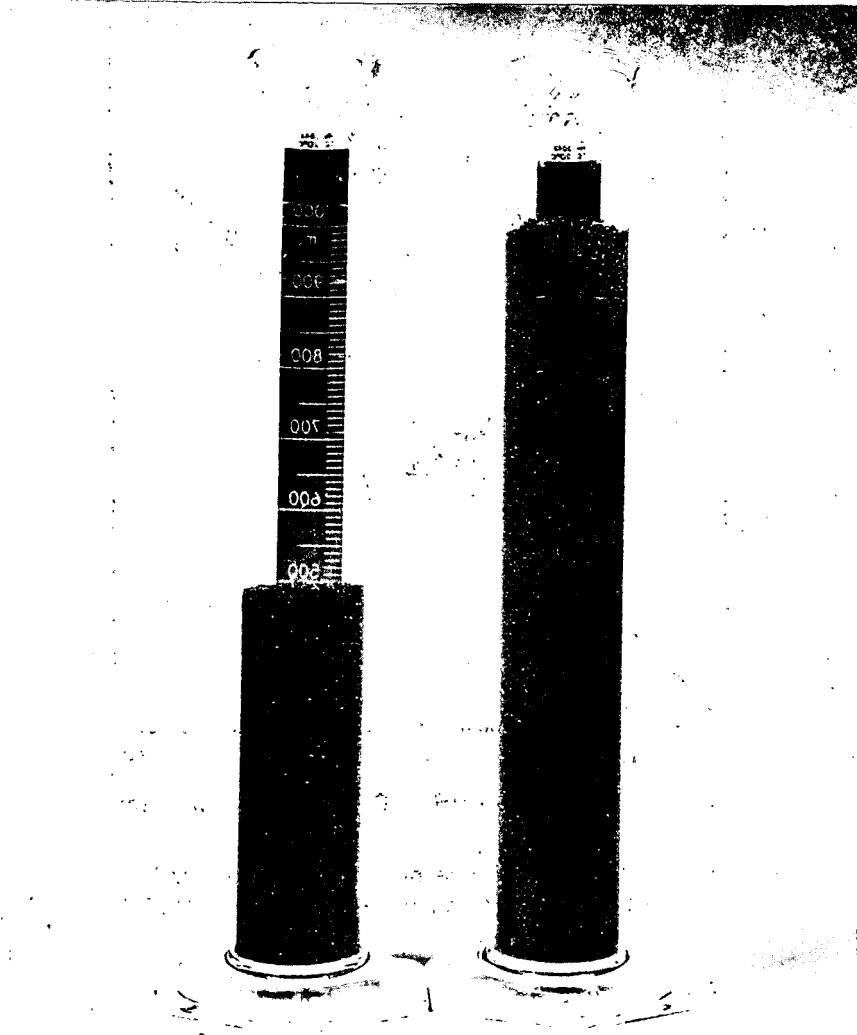


Figure 4 - Effect of pressure on bulk density of dilute-phase char.

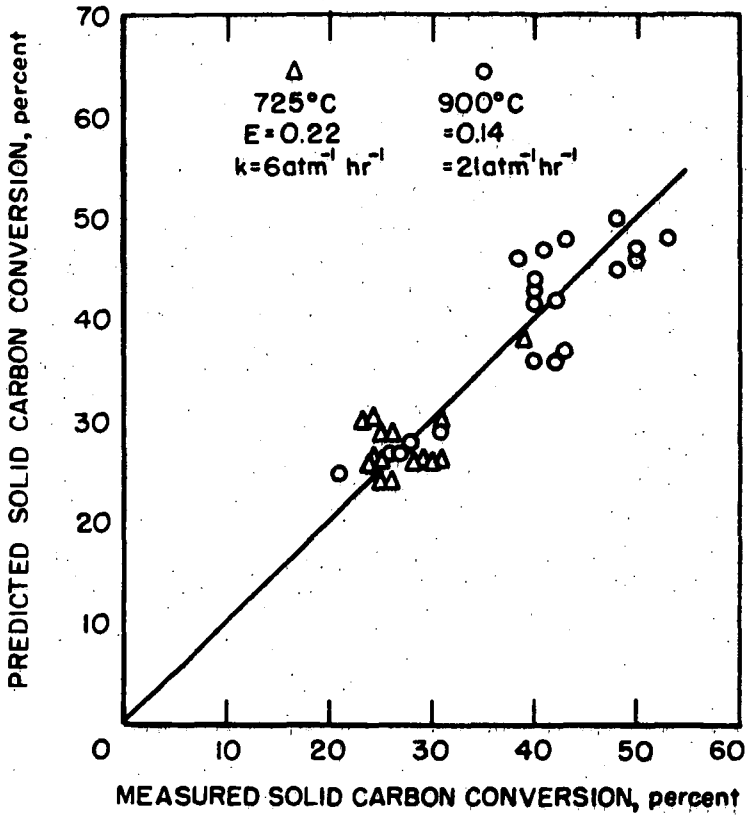


Figure 5-Prediction of average carbon conversion from reaction model at 725° and 900°C.

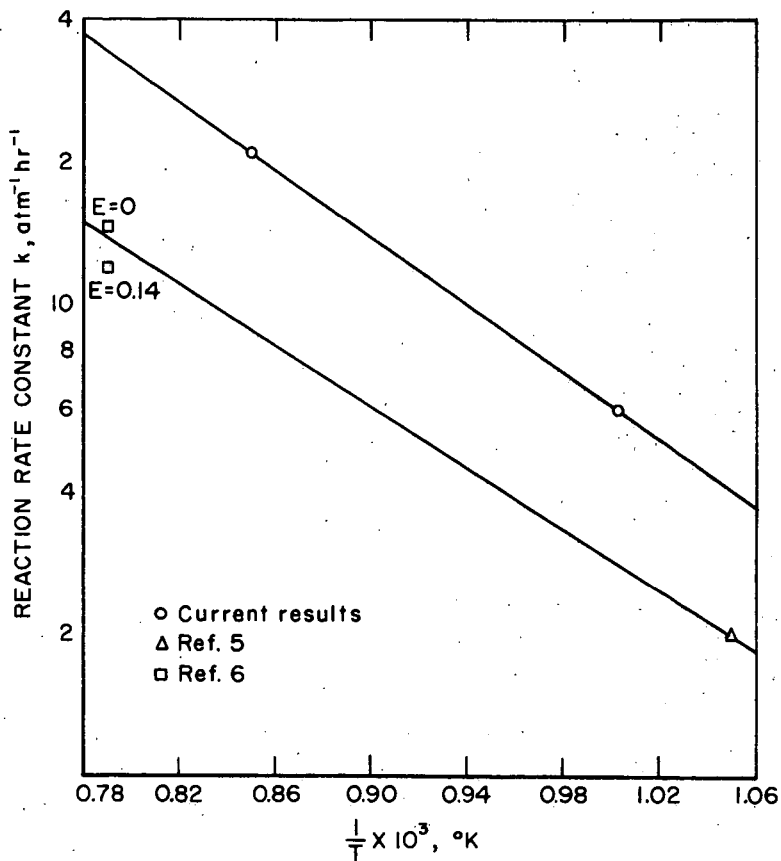


Figure 6-Effect of temperature on hydrogasification reaction rate constant.

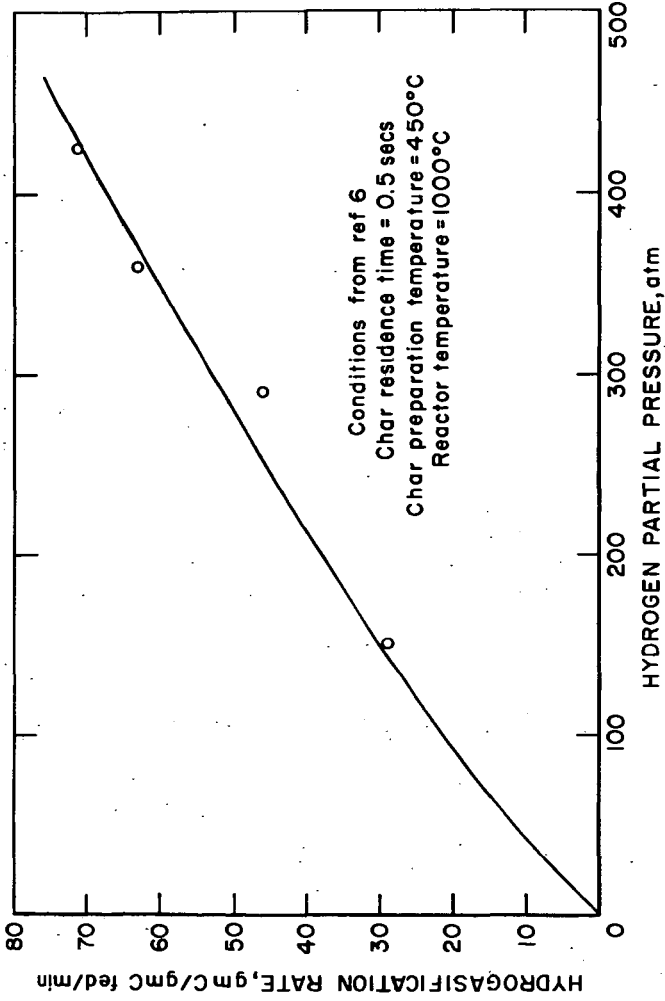


Figure 7 - Comparison of predicted char hydrogasification rate with that measured by Moseley and Paterson (6).

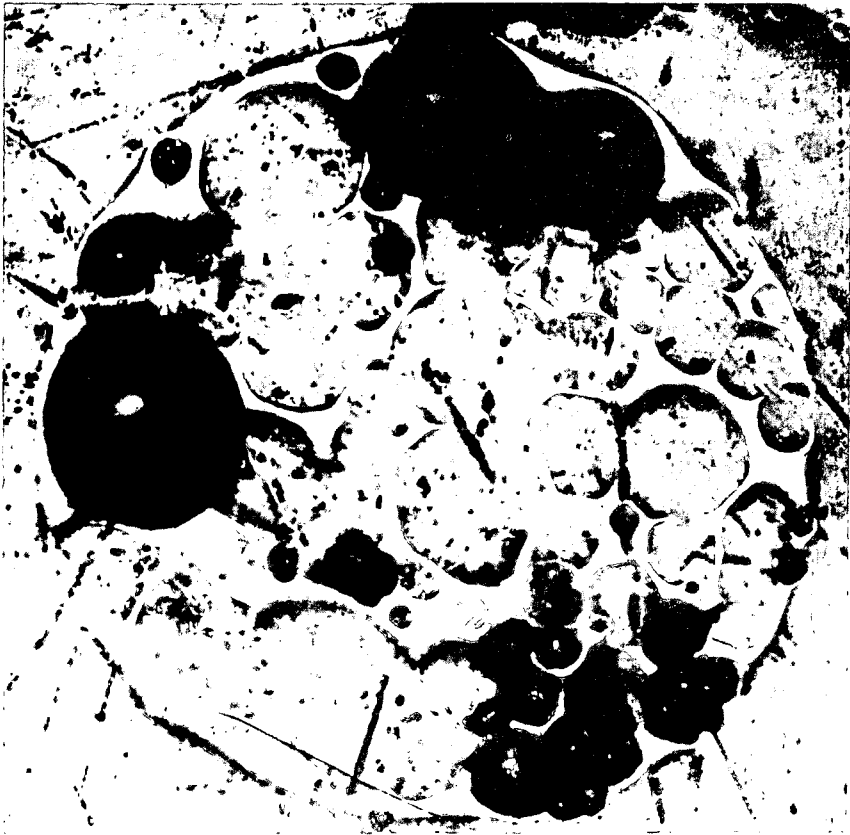


Figure 8-Cross section of char particle  
at 220 magnification.

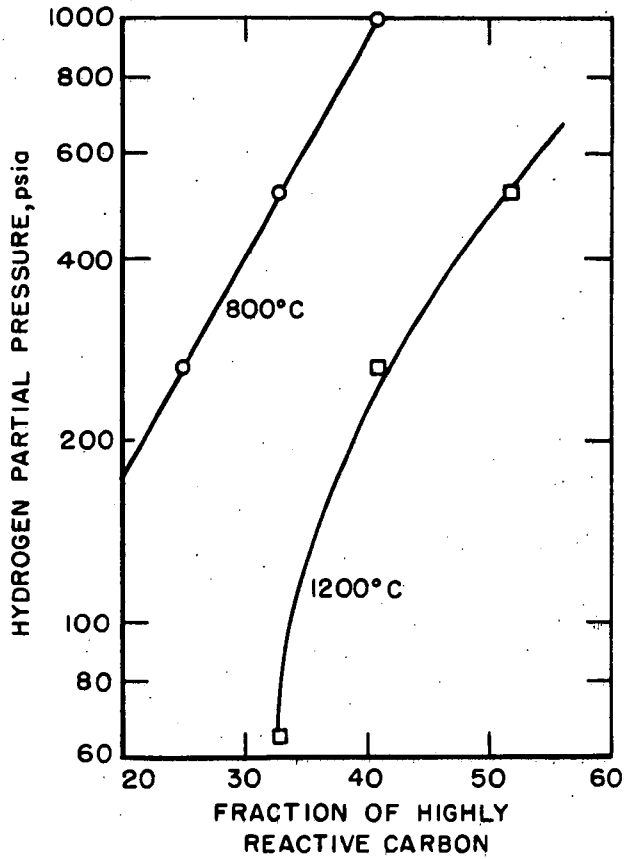


Figure 9 - Effect of hydrogen partial pressure and reaction temperature on carbon reactivity correlated from data presented by Hiteshue et al (8).

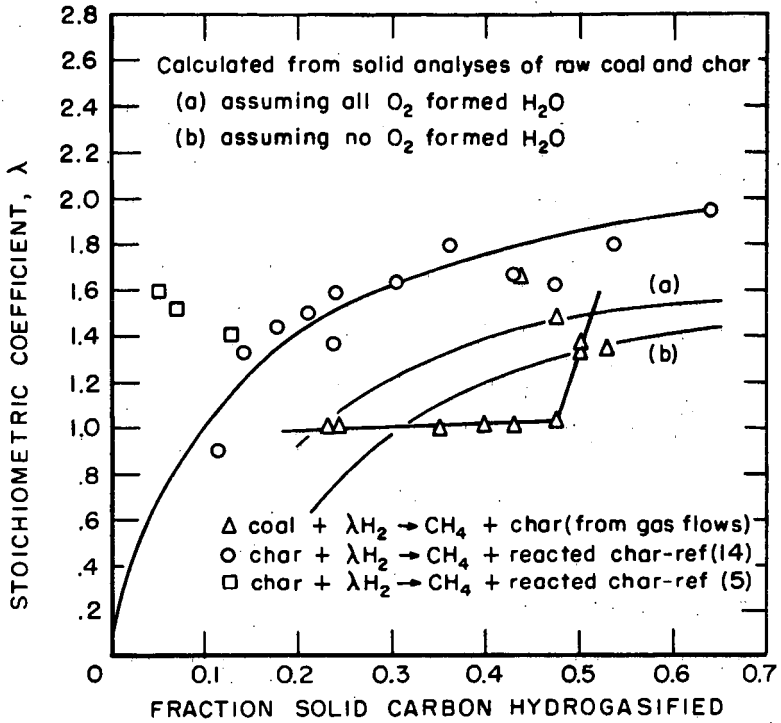


Figure 10-Dependence of the average stoichiometric coefficient for the hydrogasification of coal and char on carbon conversion level.

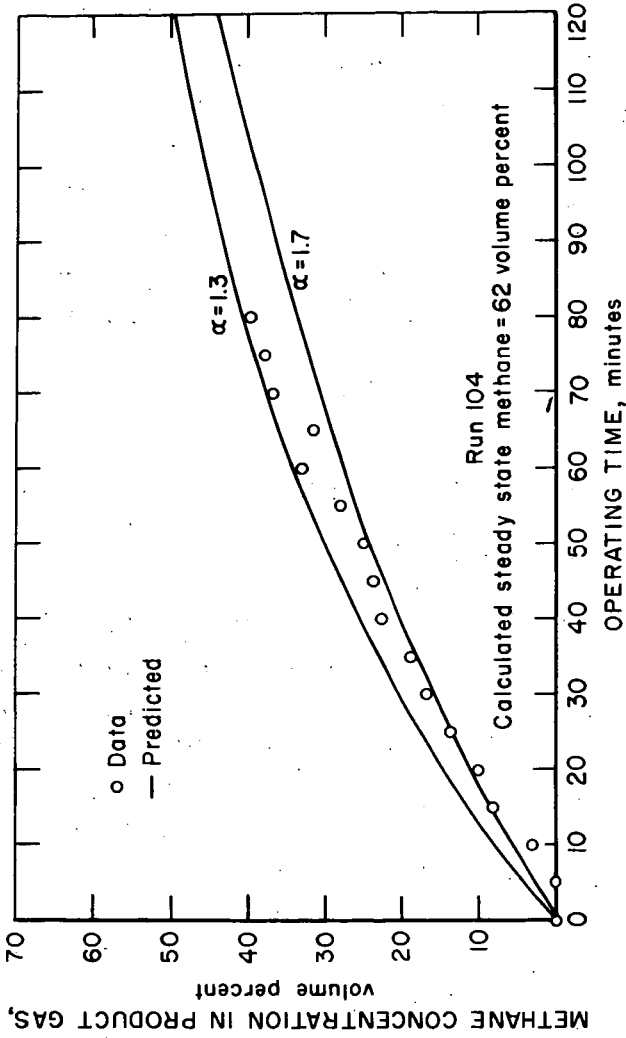


Figure 11- Transient hydrogasifier behavior with hydrogen feed gas at 900°C and 205 atm total pressure.

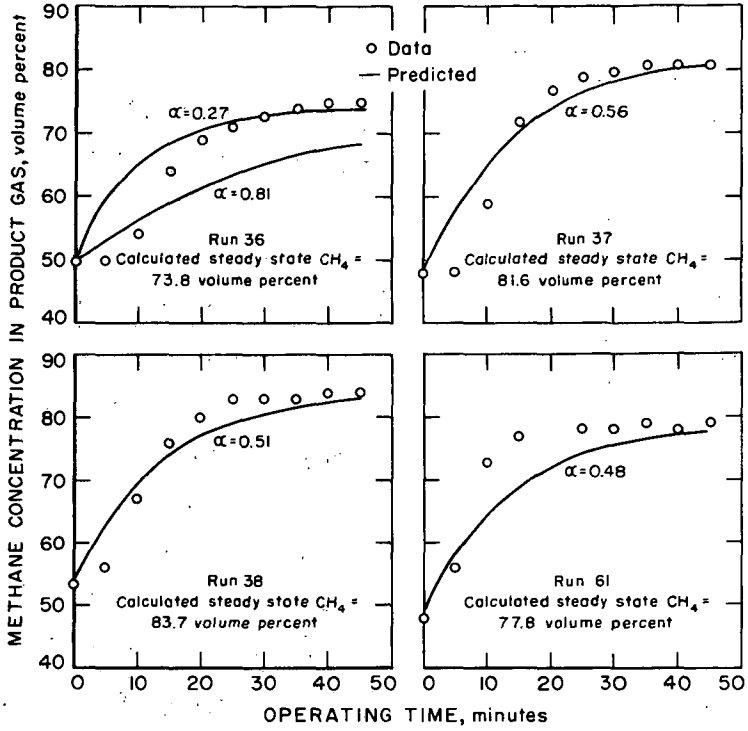


Figure 12- Transient hydrogasifier behavior with methane-hydrogen feed gas at 900°C and 205 atm total pressure.